Electronic Supplementary Information (ESI)

9.0% Power Conversion Efficiency from Ternary All-Polymer Solar Cells

Zhaojun Li, Xiaofeng Xu,* Wei Zhang, Xiangyi Meng, Zewdneh Genene, Wei Ma, Wendimagegn Mammo, Arkady Yartsev, Mats. R. Andersson, René A. J. Janssen* and Ergang Wang*

* Corresponding authors: *X. Xu*, e-mail: xixu@chalmers.se
R. A. J. Janssen, e-mail: r.a.j.janssen@tue.nl
E. Wang, e-mail: ergang@chalmers.se

Table of Contents

1. Materials

Polymer PBDTTS-FTAZ and PNDI-T10 were prepared according to our previous reports.[1,2]

Polymer PTB7-Th was purchased from Solarmer Materials, Inc.

Table S1. Number-average (M_n) and weight-average (M_w) molecular weights and polydispersity indexes (PDI) of the polymers.

Polymer	M_n (kDa)	M_w (kDa)	PDI
PBDTTS-FTAZ	22.6	72.3	3.2
PTB7-Th	35.0	105.0	3.0
PNDI-T10	66.6	333.0	5.0

2. Polymer characterization

GPC was carried out on an Agilent PL-GPC 220 Integrated High Temperature GPC/SEC System with refractive index and viscometer detectors using 3×PLgel 10 μm MIXED-B LS, 300×7.5 mm columns. The eluent was 1,2,4-trichlorobenzene at 150 °C. The molecular weights were calculated according to relative calibration with polystyrene standards. Differential scanning calorimetry (DSC) was carried out on a METTLER TOLEDO differential scanning calorimeter DSC 2, from 0 °C to 300 °C at a heating and cooling rate of 10 °C/min under N_2 flow. UV-vis-NIR absorption spectra were measured with a PerkinElmer Lambda 900 UV-Vis-NIR absorption spectrometer. Square wave voltammetry (SWV) measurements were carried out on a CH-Instruments 650A Electrochemical Workstation. PL spectra were recorded by using an Andor spectrometer (Shamrock SR-303i, coupled to a Newton EMCCD detector).

3. Differential scanning calorimetry (DSC) measurements

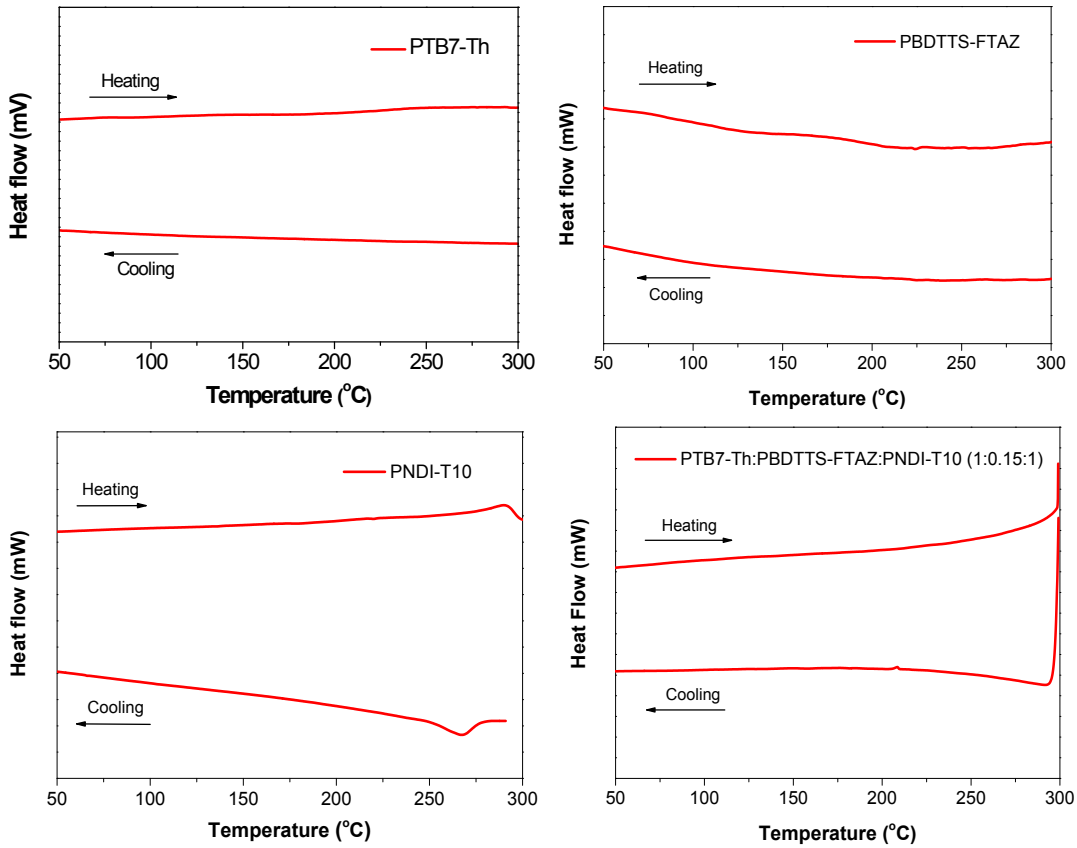

Figure S1. DSC traces of the neat polymers and ternary blend.

4. Electrochemical properties

Square wave voltammetry (SWV) measurements were carried out on a CH-Instruments 650A Electrochemical Workstation. A 0.1 M solution of tetrabutylammonium hexafluorophosphate (Bu_4NPF_6) in anhydrous acetonitrile saturated with nitrogen was used as the supporting electrolyte. Platinum wires were used as the working and counter electrodes and Ag/Ag^+ was used as the reference electrode. Potentials were referenced to the ferrocenium/ferrocene (Fc/Fc^+) couple by using ferrocene as an internal standard. Polymer films were deposited onto the working electrode from solutions. The HOMO and LUMO levels were estimated from the peak potentials by setting the oxidative peak potential of Fc/Fc^+ *vs.* the normal hydrogen electrode (NHE) to 0.63 V, and the NHE *vs.* the vacuum level to 4.5 V.[3,4] The energy levels were calculated according to the formula HOMO = $-(E_{ox} + 5.13)$ eV and LUMO = $-(E_{red} +$

5.13) eV, where the E_{ox} and E_{red} were determined from the oxidation and reduction peaks, respectively.[5]

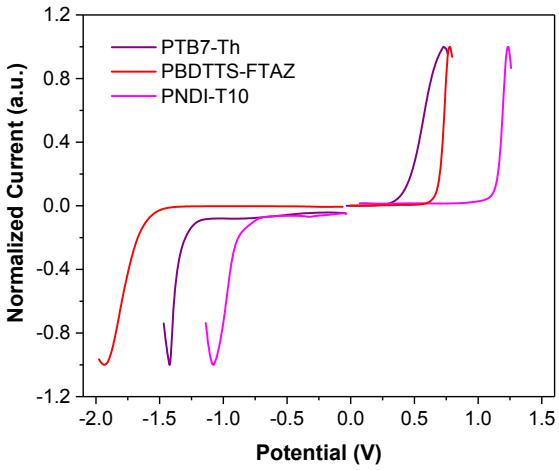

Figure S2. SWV measurements of the polymers.

5. Characterization of all-PSCs

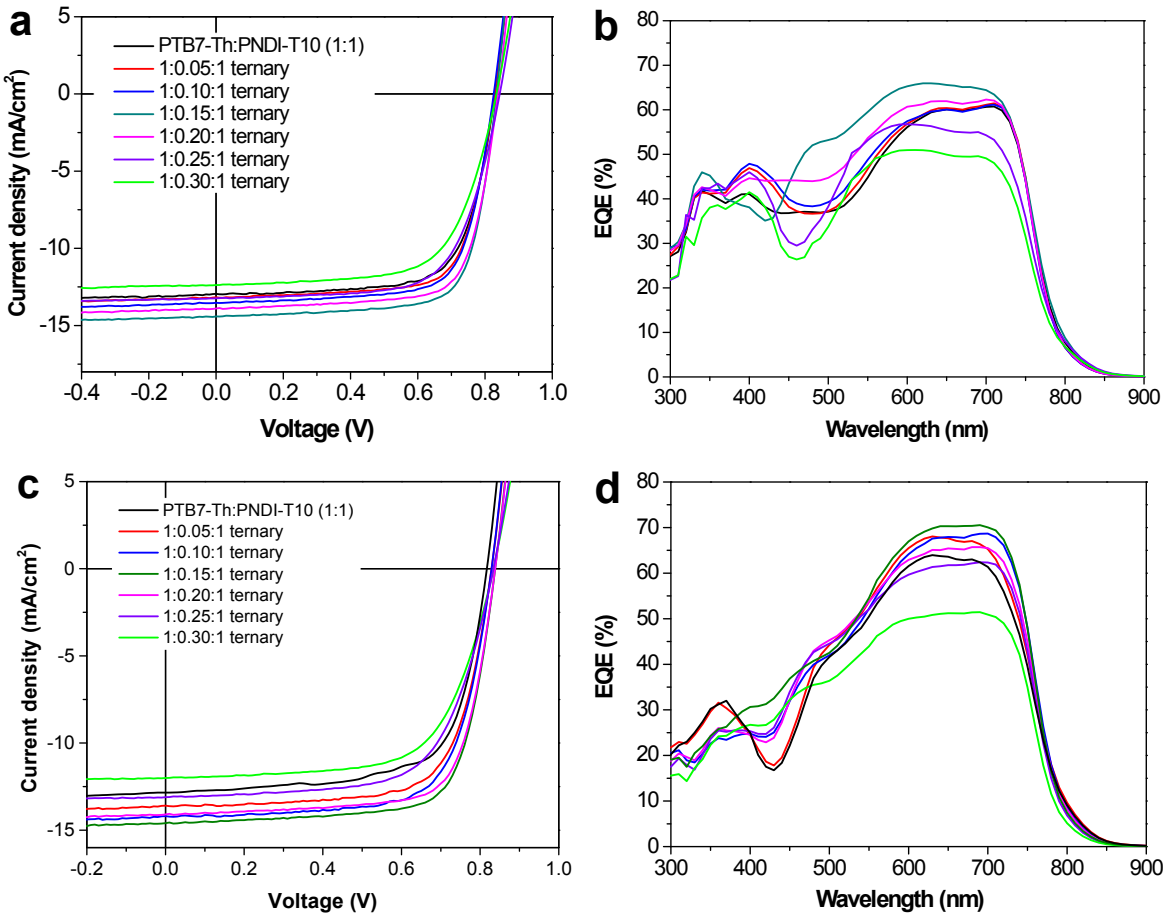

Figure S3. (a) (b) *J–V* characteristics and the corresponding EQE spectra of conventional all-PSCs; (c) (d) *J–V* characteristics and the corresponding EQE spectra of inverted all-PSCs.

Table S2. Photovoltaic performance of ten conventional ternary solar cells[a].

Blend ratio[b]	V_{oc} (V)	J_{sc} (mA/cm^2)	FF	PCE (%)
1:0.15:1	0.84	14.4	0.74	9.0
	0.84	14.2	0.74	8.8
	0.84	14.3	0.73	8.8
	0.84	14.2	0.73	8.7
	0.84	14.1	0.73	8.6
	0.84	14.0	0.73	8.6
	0.83	14.2	0.73	8.6
	0.83	14.2	0.72	8.5
	0.83	14.1	0.72	8.4
	0.83	14.0	0.72	8.4

[a] device structure: ITO/PEDOT:PSS (40 nm)/active layer/LiF (1 nm)/Al (100 nm)
[b] PTB7-Th:PBDTTS-FTAZ:PNDI-T10 = 1:0.15:1

Table S3. Photovoltaic performance of ten inverted ternary solar cells[a].

Blend ratio[b]	V_{oc} (V)	J_{sc} (mA/cm^2)	FF	PCE (%)
1:0.15:1	0.84	14.6	0.73	9.0
	0.84	14.4	0.73	8.8
	0.84	14.4	0.72	8.7
	0.83	14.5	0.72	8.7
	0.84	14.1	0.73	8.6
	0.83	14.1	0.73	8.5
	0.83	14.0	0.72	8.4
	0.83	14.2	0.71	8.4
	0.83	14.1	0.71	8.3
	0.83	13.9	0.72	8.3

[a] device structure: ITO/ZnO (40 nm)/active layer/MoO_3 (10 nm)/Ag (100 nm)
[b] PTB7-Th:PBDTTS-FTAZ:PNDI-T10 = 1:0.15:1

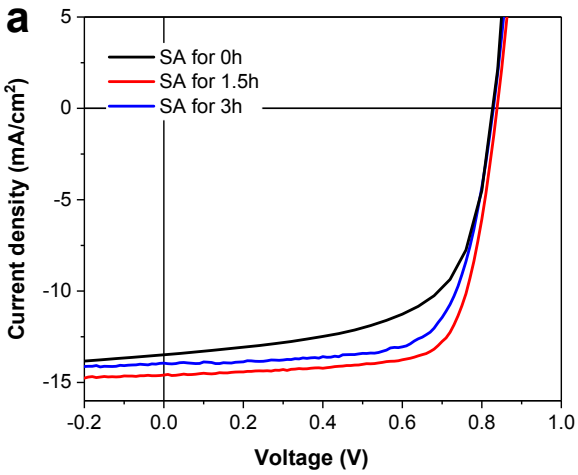

Figure S4. *J*–*V* characteristics of the conventional all-PSCs with different time of solvent annealing. (The active layers were solvent annealed under CB atmosphere with different time before evaporating the electrode.)

Table S4. Photovoltaic performance of the conventional all-PSCs with different time of solvent annealing[a].

Blend ratio[b]	Solvent annealing (hours)	V_{oc} (V)	J_{sc} (mA/cm^2)	FF	PCE (%)
	0	0.83	13.6	0.62	7.0
1:0.15:1	1.5	0.84	14.4	0.74	9.0
	3.0	0.83	13.9	0.71	8.2

[a] device structure: ITO/PEDOT:PSS (40 nm)/active layer/LiF (1 nm)/Al (100 nm)
[b] PTB7-Th:PBDTTS-FTAZ:PNDI-T10 = 1:0.15:1

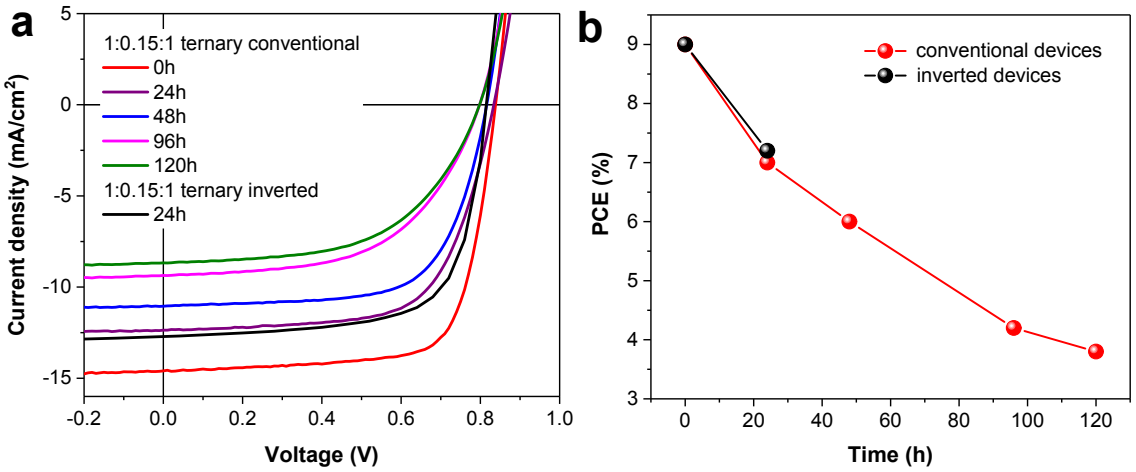

Figure S5. (a) *J*–*V* characteristics of the 1:0.15:1 ternary all-PSCs with different storage time. (The active layer was solvent annealed under CB atmosphere for 1.5 h before evaporating the electrode, and then the unencapsulated device was stored in the glove box at 20 °C with different time.) (b) Corresphonding PCEs as a function of the storage time in the 1:0.15:1 ternary all-PSCs. (The PCEs were measured from the same device for the conventional or inverted solar cells.)

Table S5. Photovoltaic performance of the all-PSCs with different storage time.

Blend ratio[a]	Storage time (hours)	V_{oc} (V)	J_{sc} (mA/cm^2)	FF	PCE (%)
1:0.15:1[b]	0	0.84	14.4	0.74	9.0
	24	0.83	12.8	0.66	7.0
	48	0.82	11.0	0.67	6.0
	96	0.80	9.4	0.56	4.2
	120	0.80	8.7	0.55	3.8
1:0.15:1[c]	0	0.84	14.6	0.73	9.0
	24	0.82	12.7	0.69	7.2

[a] PTB7-Th:PBDTTS-FTAZ:PNDI-T10 = 1:0.15:1
[b] device structure: ITO/PEDOT:PSS (40 nm)/active layer/LiF (1 nm)/Al (100 nm)
[c] device structure: ITO/ZnO (40 nm)/active layer/MoO_3 (10 nm)/Ag (100 nm)

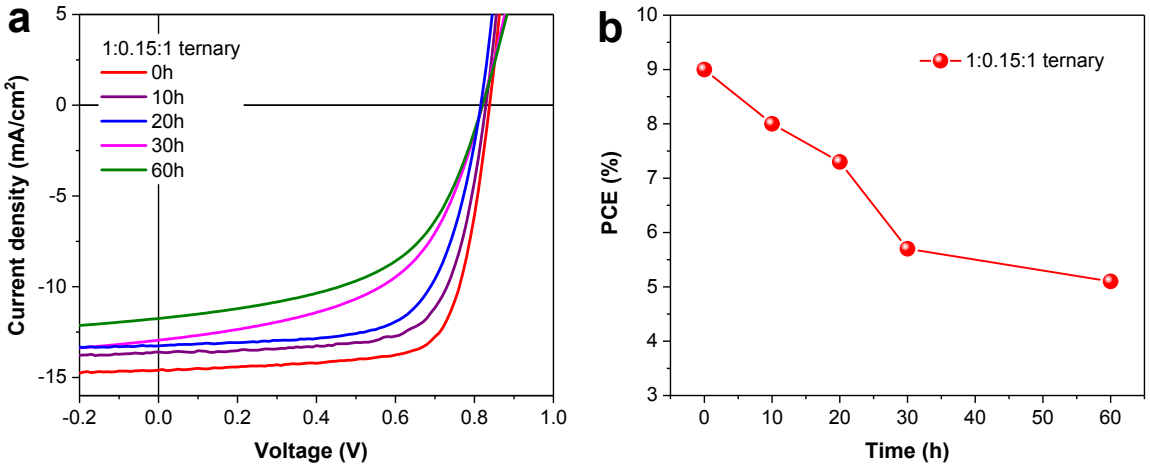

Figure S6. *J–V* characteristics of the conventional all-PSCs with different time of thermal annealing at 80 °C. (Before evaporating the electrode, all the active layers were solvent annealed under CB atmosphere for 1.5 h, and then the active layers were thermal annealed at 80 °C with different time in the glove box.) (b) Corresphonding PCEs as a function of the thermal annealing time in the conventional all-PSCs.

Table S6. Photovoltaic performance of the conventional all-PSCs with different time of thermal annealing at 80 °C[a].

Blend ratio[b]	Thermal annealing (hours)	V_{oc} (V)	J_{sc} (mA/cm^2)	FF	PCE (%)
1:0.15:1	0	0.84	14.4	0.74	9.0
	10	0.83	13.6	0.71	8.0
	20	0.82	13.2	0.67	7.3
	30	0.82	12.9	0.54	5.7
	60	0.82	11.7	0.53	5.1

[a] device structure: ITO/PEDOT:PSS (40 nm)/active layer/LiF (1 nm)/Al (100 nm)
[b] PTB7-Th:PBDTTS-FTAZ:PNDI-T10 = 1:0.15:1

6. Space charge limited current (SCLC) mobilities

The hole mobility was measured in a hole-only device composed of ITO/PEDOT:PSS/active layer/Au. The electron mobility was measured in an electron-only device composed of ITO/ZnO/active layer/LiF/Al. For the hole-only device, the blend films were spin-coated on ITO substrates covered with 40 nm PEDOT:PSS. The polymer solutions (12 mg/mL) in CB were spin-coated at 1000 rpm for 60 s. After that, Au (100 nm) was vacuum-deposited on the active layer as the cathode. For the electron-only device, the blend films were spin-coated on ITO substrates covered with a layer of ZnO (40 nm). Solutions of the polymer blends (12 mg/mL) in CB were spin-coated at 1000 rpm for 60 s. After that, 100 nm Al was vacuum-deposited on the active layer as the cathode. The mobility μ was determined by fitting the dark current to the model of a single carrier SCLC, which is described by Equation (S1):

$$J = \frac{9}{8}\varepsilon_0\varepsilon_r\mu\frac{V^2}{d^3} \qquad \text{(S1)}$$

where J is the current density, μ is the charge (hole or electron) mobility at zero field, ε_0 is the free-space permittivity, ε_r is the relative permittivity of the material, d is the thickness of the active layer, and V is the effective voltage $V–V_{bi}$. The charge (hole or electron) mobilities are calculated from the y-intercept of the $J–V$ curves.

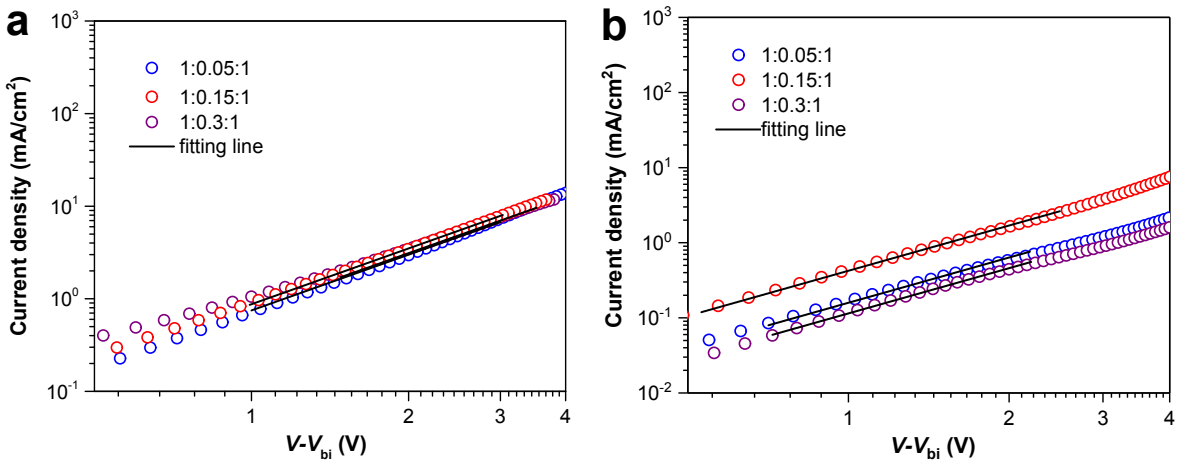

Figure S7. (a) Current density–voltage and SCLC fitting curves of the ternary blends with the hole-only device structure of ITO/PEDOT:PSS(40 nm)/active layer/Au(100 nm). (b) Current

density–voltage and SCLC fitting curves of the ternary blends with electron-only device structure of ITO/ZnO(40 nm)/active layer/LiF(1 nm)/Al(100 nm).

Table S7. SCLC mobilities of the ternary blends.

D_1:D_2:A[a]	μ_h [b] [$cm^2\ V^{-1}\ s^{-1}$]	μ_e [c] [$cm^2\ V^{-1}\ s^{-1}$]	μ_h/μ_e
1:0.05:1	8.4×10^{-4}	5.2×10^{-4}	1.6
1:0.15:1	8.9×10^{-4}	6.2×10^{-4}	1.4
1:0.3:1	8.3×10^{-4}	1.4×10^{-4}	6.0

[a] D_1 is PTB7-Th; D_2 is PBDTTS-FTAZ; A is PNDI-T10

7. Estimation of individual absorption of neat polymers in the blend

The absorption spectrum of the blend can be simulated by a linear combination of the corresponding absorption spectra of the neat donor and acceptor films, as described by Equation S2,[6,7]

$$A_B(\lambda) = C_D A_D(\lambda) + C_A A_A(\lambda) \qquad \text{(S2)}$$

where $A_B(\lambda)$ is absorbance of the blend film, $A_D(\lambda)$ and $A_A(\lambda)$ are absorbance of the neat donor and acceptor films, C_D and C_A are the contributions of the donor and acceptor absorbance in the blend, respectively. In this scenario, we neglected the interference effects and contribution from the ground-state charge-transfer complex,[8,9] and assumed that the absorption spectra of the donor and acceptor in the blend film are similar with those in their neat films. Thus, we could estimate the individual absorption curve of each polymer in the blend.

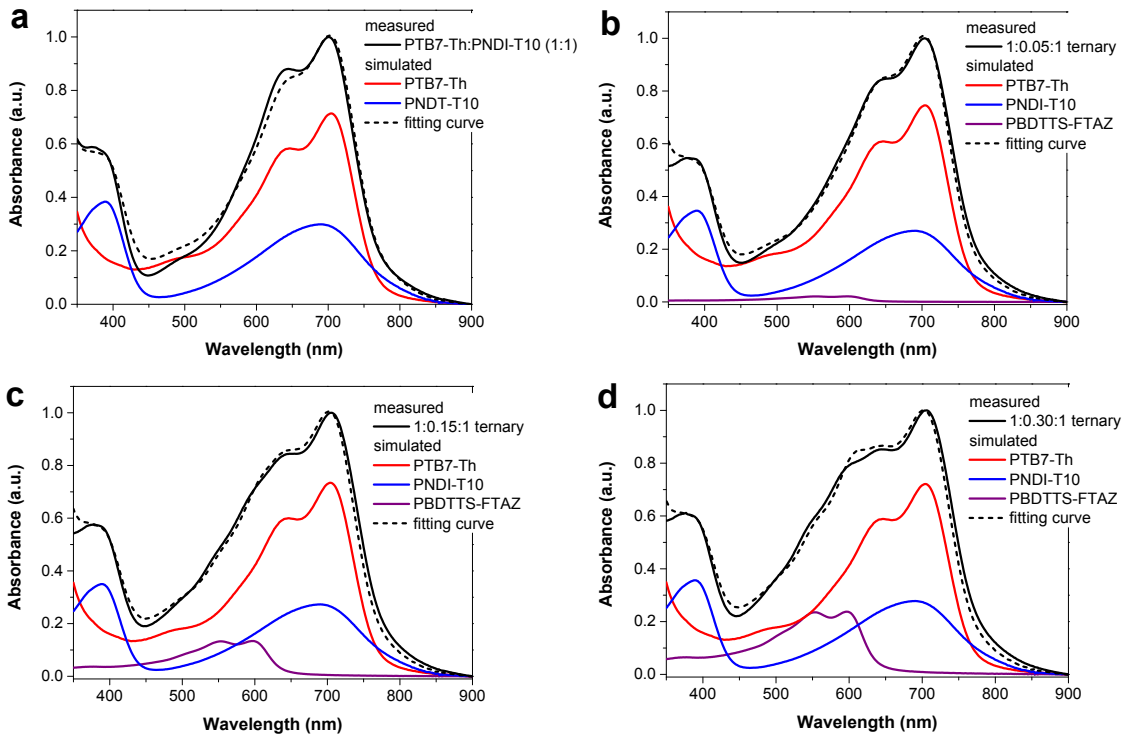

Figure S8. Simulated absorbance of the neat polymer films and the fitting curves of the blend films.

Table S8. Summary of the contribution of the polymer to the absorption of the blend film at the excitation wavelength of 532 nm

D_1:D_2:A[a]	$R_{PBDTTS-FTAZ}$	$R_{PTB7-Th}$	$R_{PNDI-T10}$
1:0:1	–	74%	26%
1:0.05:1	6%	72%	22%
1:0.15:1	29%	54%	17%
1:0.30:1	43%	43%	14%

[a]D_1 is PTB7-Th; D_2 is PBDTTS-FTAZ; A is PNDI-T10

8. Photoluminescence (PL) quenching measurements

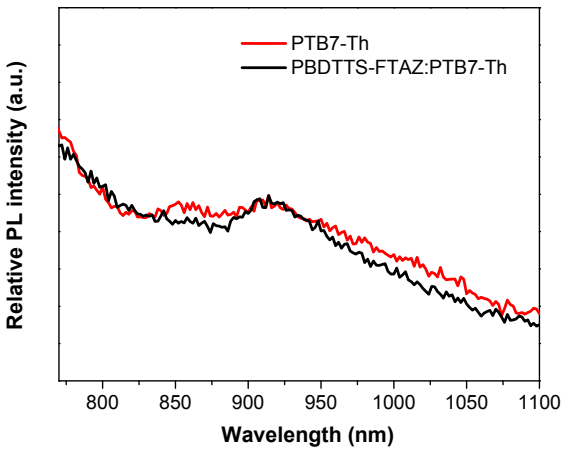

Figure S9. PL spectra of the neat PTB7-Th and PTB7-Th:PBDTTS-FTAZ binary films excited at 700 nm.

9. Time-resolved photoluminescence (TRPL) measurements

A Ti:Sapphire laser (Spectra-Physics, Tsunami) at 800 nm was used as an excitation source with repetition rate of 80 MHz and pulse duration of 100 fs and a frequency-doubled light (400 nm, generated by Photop Technologies, Tripler TP-2000B) was used for excitation. Two 1-inch quartz plano-convex lenses of 50 mm focal length were used to collect PL and focused on the input slit of a spectrograph (Chromex). A streak camera (Hamamatsu C6860) with a slit width of 20 μm was used to collect the output of the spectrograph. Background correction of the measured PL images was performed first and then the shading and spectral sensitivity correction of the fluorescence spectrometer was carried out with calibrated reference light source (Ocean Optics, LS-1-CAL). All measurements were carried out at room temperature.

10. Atomic force microscopy (AFM) measurements

Tapping-mode atomic force microscopy (AFM) images were acquired with an ND-MDT NTEGRA Prima scanning probe microscope in the AEK-2002 acoustic enclosure, using ND-MDT NSG01/50 tips and resonant frequencies of 300 kHz.

AFM sample preparation: PEDOT:PSS was spin-coated onto the ITO glass at a spin-coating rate of 3000 rpm for 60 s, followed by annealing at 150 °C for 10 minutes. The active layers were spin-coated from warm CB solution onto the PEDOT:PSS layer in a glove box.

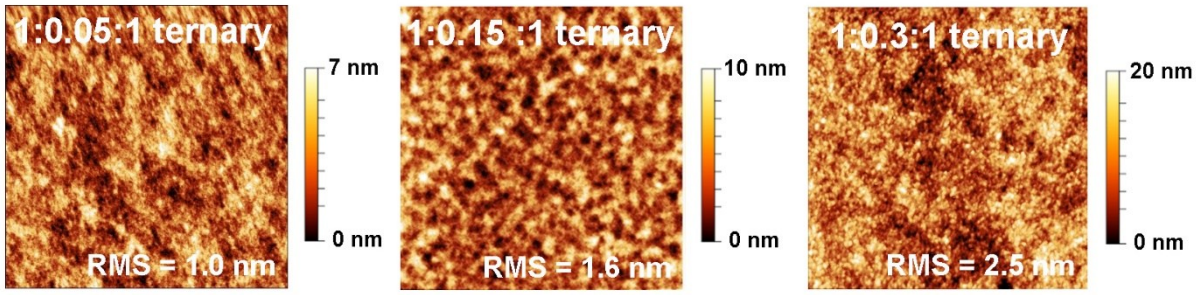

Figure S10. AFM topography (5×5 μm^2) images of the ternary blend films with different loading of PBDTT-FTAZ. (All the blend fims were solvent annealed under CB atmosphere for 1.5 h.)

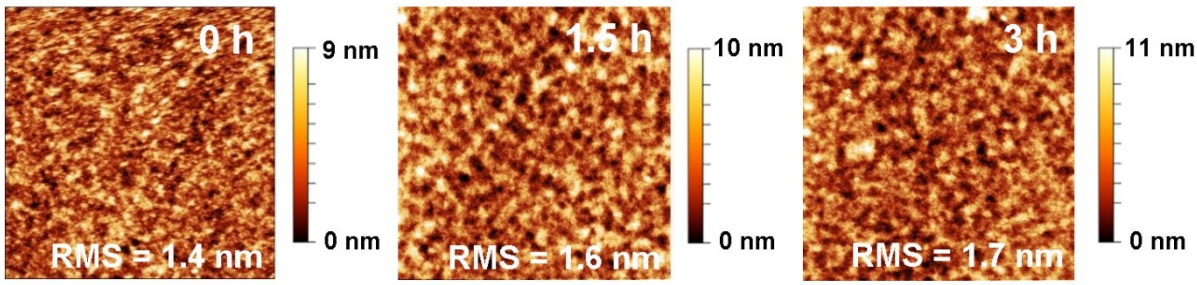

Figure S11. AFM topography (5×5 μm^2) images of the 1:0.15:1 ternary blend films with different time of solvent annealing. (All the blend films were solvent annealed under CB atmosphere with different time in the glove box.)

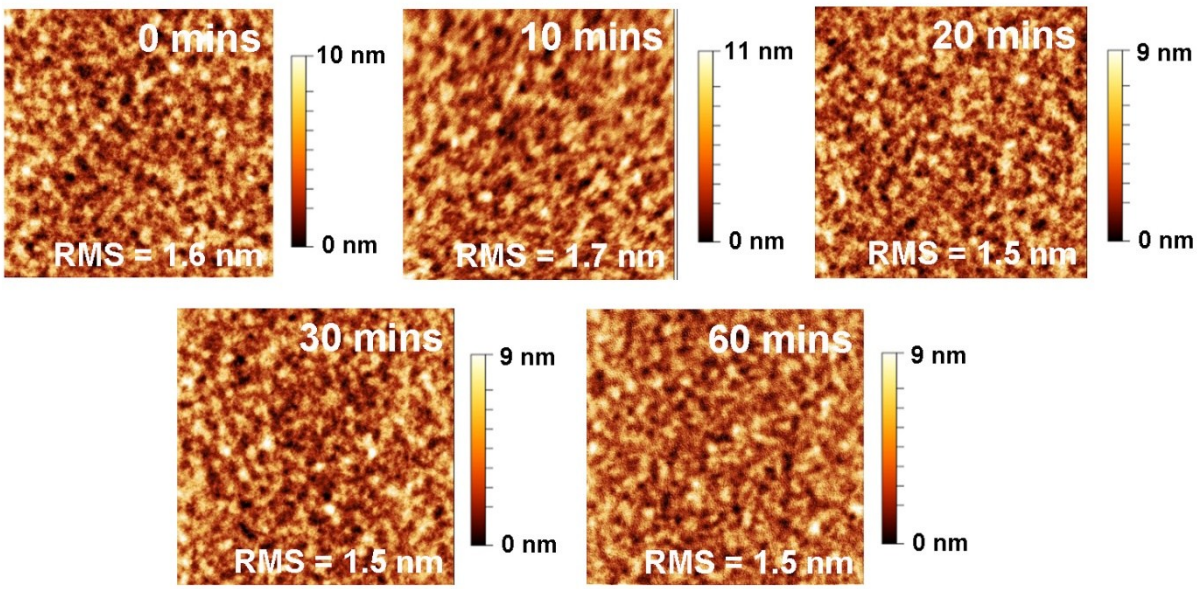

Figure S12. AFM topography (5×5 μm^2) images of the 1:0.15:1 ternary blend films with different time of thermal annealing at 80 °C. (All the blend films were solvent annealed under CB atmosphere for 1.5 h. and then the blend films were thermal annealed at 80 °C with different time in the glove box.)

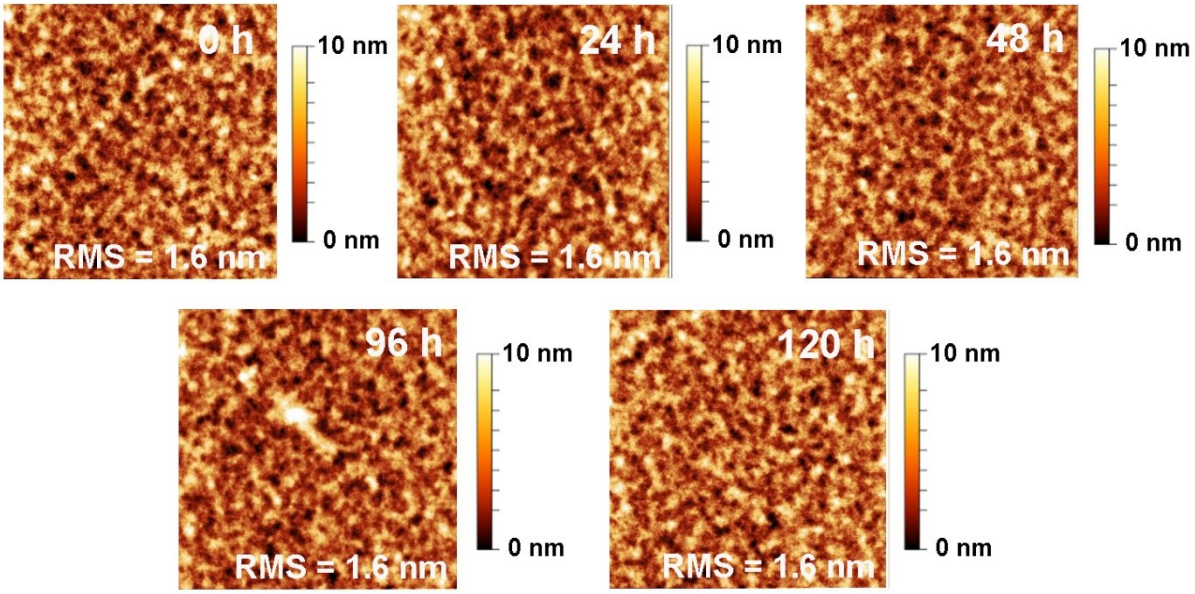

Figure S13. AFM topography (5×5 μm^2) images of the 1:0.15:1 ternary blend film with different storage time. (All the blend film was solvent annealed under CB atmosphere for 1.5 h, and then the blend film was stored in the glove box at 20 °C with different time. The AFM images were measured from the same film.)

11. Grazing incidence wide-angle X-ray scattering (GIWAXS) measurements

Grazing incidence X-ray scattering characterization of the thin films was performed at the Advanced Light Source (ALS) on beam 7.3.3.[10] The 10 KeV X-ray beam was incident at a grazing angle of 0.10–0.15°, which optimized signal-to-background ratio. The data was processed and analyzed using the NIKA software package.

Table S9. Summary of polymer packing parameters at the in-plane direction

Direction	Blend ratio[a]	Lamellar stack PTB7-Th (100)				Lamellar stack PNDI-T10 (100)			
		Scattering vector (q) [Å^{-1}]	d-spacing [nm]	FWHM[b]	CL (nm)	Scattering vector (q) [Å^{-1}]	d-spacing [nm]	FWHM	CL (nm)
In-plane	1:0:1	0.27	2.30	0.149	3.79	0.26	2.43	0.070	8.03
	1:0.05:1	0.28	2.24	0.146	3.86	0.26	2.37	0.069	8.17
	1:0.15:1	0.28	2.24	0.154	3.68	0.26	2.38	0.070	8.08
	1:0.30:1	0.28	2.23	0.148	3.81	0.26	2.37	0.072	7.85

[a] PTB7-Th:PBDTTS-FTAZ:PNDI-T10
[b] FWHM is full width at half maximum of the scattering peak.

Table S10. Summary of polymer packing parameters in the out-of-plane direction

Direction	π-π stack (010)				
	Blend ratio[a]	Scattering vector (q) [Å^{-1}]	d-spacing [nm]	FWHM[b]	CL (nm)
Out-of-plane	1:0:1	1.58	0.397	0.307	1.84
	1:0.05:1	1.59	0.395	0.358	1.58
	1:0.15:1	1.61	0.391	0.395	1.43
	1:0.30:1	1.61	0.389	0.388	1.45

[a] PTB7-Th:PBDTTS-FTAZ:PNDI-T10
[b] FWHM is full width at half maximum of the scattering peak.

12. *J–V* characteristics under reverse bias voltages

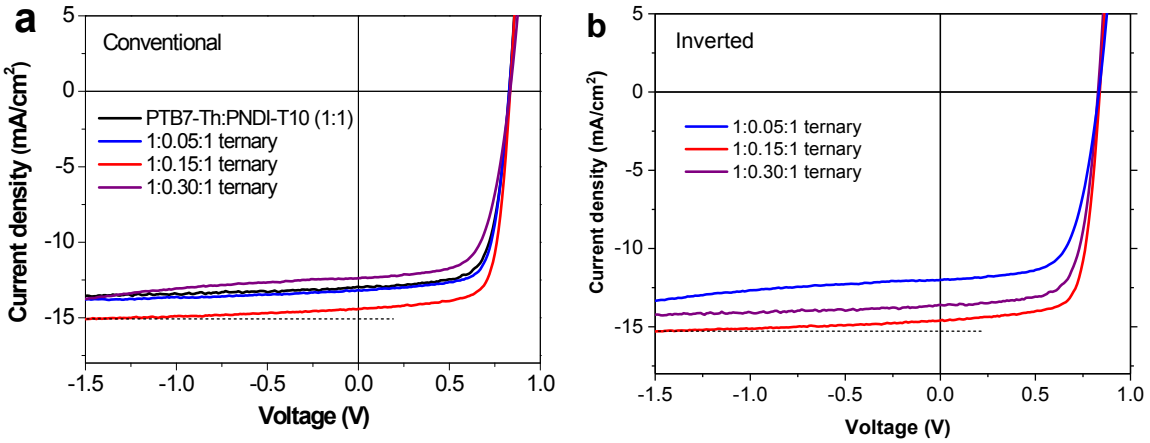

Figure S14. *J–V* curves of the binary and ternary all-PSCs under reverse bias voltages.

13. EQE characteristics under bias light

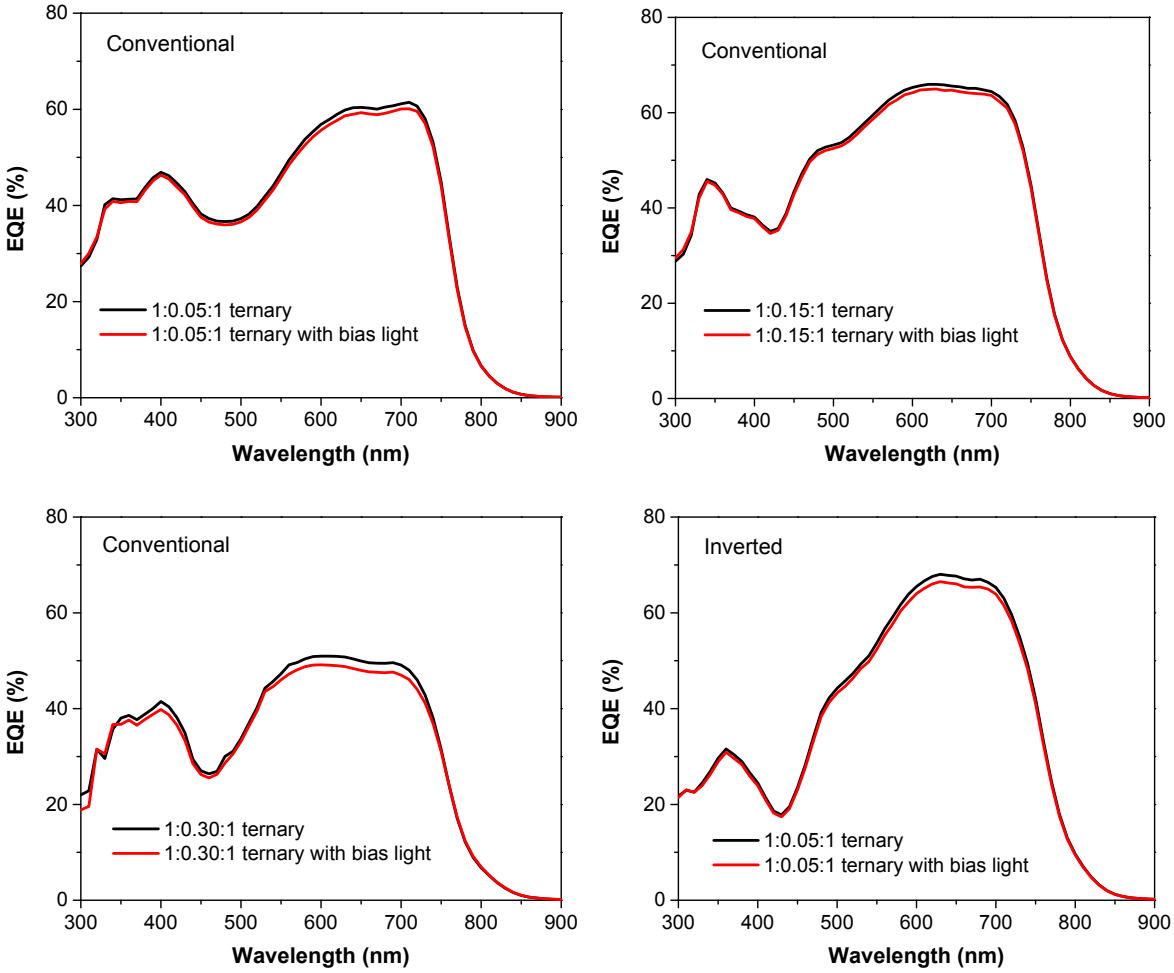

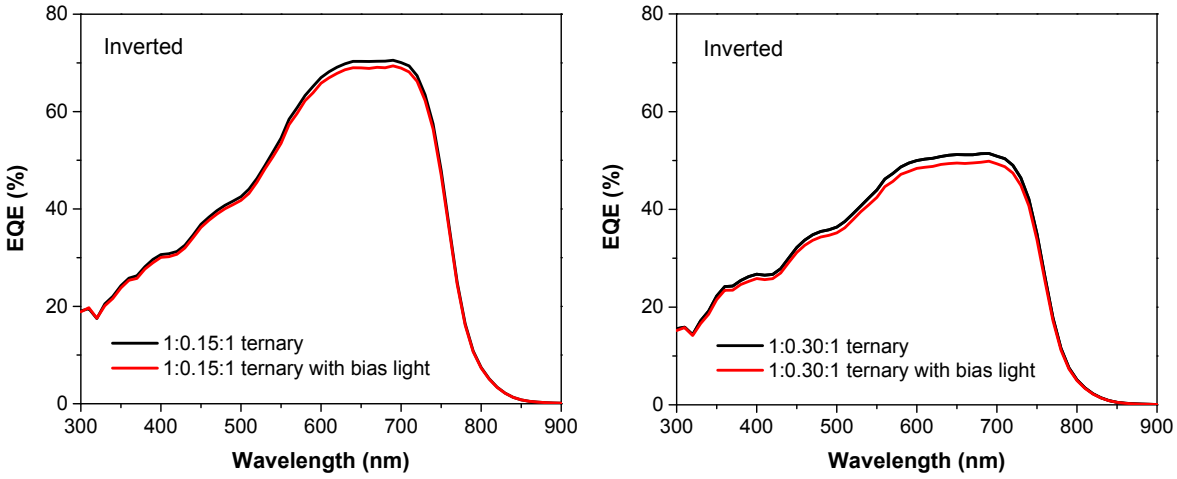

Figure S15. EQE curves of the ternary all-PSCs with and without bias light.

14. Internal quantum efficiency (IQE) calculation

The absorbance, transmittance and reflection of each functional layer were taken into account. The refractive index *n*, extinction coefficient *k* of the blend films were calculated from the transmittance and reflection measurements. Using a transfer matrix formalism (TMF), the absorptance spectra of the active layers were calculated with a device configuration of Glass (100 nm)/SiO_2 (20 nm)/ITO (170 nm)/PEDOT:PSS (40 nm)/active layer (95 nm)/Al (100 nm). The *n* and *k* values of the glass substrate, charge transporting layers and electrodes were included as input to simulate the absorption distribution in the actual devices.

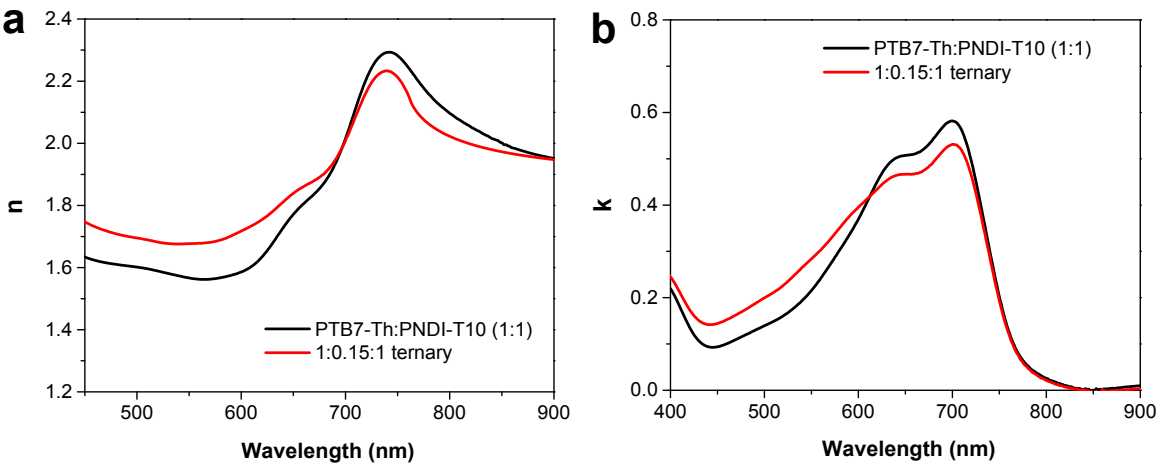

Figure S16. (a) *n* curve, and (b) *k* curve of the PTB7-Th:PNDI-T10 binary and ternary blends.

15. References

1. Z. Genene, J. Wang, X. Meng, W. Ma, X. Xu, R. Yang, W. Mammo, E. Wang, *Adv. Electron. Mater*. 2016, **2**, 1600084.
2. Z. Li, X. Xu, W. Zhang, X. Meng, W. Ma, A. Yartsev, O. Inganäs, M. R. Andersson, R. A. J. Janssen, E. Wang, *J. Am. Chem. Soc*. 2016, **138**, 10935.
3. V. V. Pavlishchuk, A. W. Addison, *Inorg. Chim. Acta* 2000, **298**, 97.
4. A. J. Bard, L. R. Faulkner, *Electrochemical Methods: Fundamentals and Applications*, Wiley, 2000.
5. C. M. Cardona, W. Li, A. E. Kaifer, D. Stockdale, G. C. Bazan, *Adv. Mater*. 2011, **23**, 2367.
6. Z. Li, X. Xu, W. Zhang, Z. Genene, W. Mammo, A. Yartsev, M. R. Andersson, R. A. J. Janssen, E. Wang, *J. Mater. Chem. A*, 2017, **5**, 11693-11700.
7. Z. Li, W. Zhang, X. Xu, Z. Genene, D. D. Carlo Rasi, W. Mammo, A. Yartsev, M. R. Andersson, R. A. J. Janssen, E. Wang, *Adv. Energy Mater*. 2017, **7**, 1602722.
8. J. J. Benson-Smith, L. Goris, K. Vandewal, K. Haenen, J. V. Manca, D. Vanderzande, D. D. C. Bradley, J. Nelson, *Adv. Funct. Mater*. 2007, **17**, 451.
9. K. Vandewal, S. Albrecht, E. T. Hoke, K. R. Graham, J. Widmer, J. D. Douglas, M. Schubert, W. R. Mateker, J. T. Bloking, G. F. Burkhard, A. Sellinger, J. M. J. Fréchet, A. Amassian, M. K. Riede, M. D. McGehee, D. Neher, A. Salleo, *Nat. Mater*., 2014, **13**, 63.
10. H. Alexander, B. Wim, G. James, S. Eric, G. Eliot, K. Rick, M. Alastair, C. Matthew, R. Bruce, P. Howard, *J. Phys. Conf. Ser*. 2010, **247**, 012007.